Journal of Cerebral Blood Flow & Metabolism (2010) 30, 994–1007

www.jcbfm.com

# High-affinity dopamine $D_2/D_3$ PET radioligands $^{18}$F-fallypride and $^{11}$C-FLB457: A comparison of kinetics in extrastriatal regions using a multiple-injection protocol

Nicholas T Vandehey[1], Jeffrey M Moirano[1], Alexander K Converse[2], James E Holden[1], Jogesh Mukherjee[3], Dhanabalan Murali[2], R Jerry Nickles[1], Richard J Davidson[2], Mary L Schneider[4] and Bradley T Christian[1,2]

[1]*Department of Medical Physics, University of Wisconsin—Madison, Madison, Wisconsin, USA;* [2]*Waisman Laboratory for Brain Imaging and Behavior, University of Wisconsin—Madison, Madison, Wisconsin, USA;* [3]*Brain Imaging Center, University of California—Irvine, Irvine, California, USA;* [4]*Department of Psychology, University of Wisconsin—Madison, Madison, Wisconsin, USA*

**$^{18}$F-Fallypride and $^{11}$C-FLB457 are commonly used PET radioligands for imaging extrastriatal dopamine $D_2/D_3$ receptors, but differences in their *in vivo* kinetics may affect the sensitivity for measuring subtle changes in receptor binding. Focusing on regions of low binding, a direct comparison of the kinetics of $^{18}$F-fallypride and $^{11}$C-FLB457 was made using a MI protocol. Injection protocols were designed to estimate $K_1$, $k_2$, $f_{ND}k_{on}$, $B_{max}$, and $k_{off}$ in the midbrain and cortical regions of the rhesus monkey. $^{11}$C-FLB457 cleared from the arterial plasma faster and yielded a ND space distribution volume ($K_1/k_2$) that is three times higher than $^{18}$F-fallypride, primarily due to a slower $k_2$ (FAL:FLB; $k_2 = 0.54\,min^{-1}$:$0.18\,min^{-1}$). The dissociation rate constant, $k_{off}$, was slower for $^{11}$C-FLB457, resulting in a lower $K_{Dapp}$ than $^{18}$F-fallypride (FAL:FLB; 0.39 nM:0.13 nM). Specific $D_2/D_3$ binding could be detected in the cerebellum for $^{11}$C-FLB457 but not $^{18}$F-fallypride. Both radioligands can be used to image extrastriatal $D_2/D_3$ receptors, with $^{11}$C-FLB457 providing greater sensitivity to subtle changes in low-receptor-density cortical regions and $^{18}$F-fallypride being more sensitive to endogenous dopamine displacement in medium-to-high-receptor-density regions. In the presence of specific $D_2/D_3$ binding in the cerebellum, reference region analysis methods will give a greater bias in $BP_{ND}$ with $^{11}$C-FLB457 than with $^{18}$F-fallypride.**
*Journal of Cerebral Blood Flow & Metabolism* (2010) **30,** 994–1007; doi:10.1038/jcbfm.2009.270; published online 30 December 2009

**Keywords:** $D_2/D_3$; dopamine; fallypride; FLB457; multiple injection; PET

## Introduction

Extrastriatal dopamine $D_2/D_3$ receptors have a functional role in normal cognitive processing, motivation regulation, and reward processing; and disruption of their circuitry may be implicated in the etiology of several neuropsychiatric disorders. The positron emission tomography (PET) radioligands $^{18}$F-fallypride and $^{11}$C-FLB457, both high-affinity $D_2/D_3$ antagonists, provide the ability to image receptors in low concentrations ($< 1$ nmol/L) and serve as valuable biomarkers for studying the dopaminergic system. For high-affinity radiotracers, longer scan times ($> 2$ h) are required for accurate assay in high-density regions, thus limiting the utility of $^{11}$C-FLB457 for striatal $D_2/D_3$ measurement (Olsson and Farde, 2001). A number of studies have been conducted to characterize the *in vivo* kinetics of these radiotracers and to evaluate experimental designs for measuring extrastriatal $D_2/D_3$ receptor binding. Of particular interest is the determination of the sensitivity of these radioligands to variations in endogenous dopamine concentrations (Mukherjee *et al*, 2005; Narendran *et al*, 2009; Okauchi *et al*, 2001; Riccardi *et al*, 2008; Slifstein *et al*, 2004b), determination of *in vivo* affinity (Christian *et al*, 2004; Mukherjee *et al*, 1999; Olsson

Correspondence: Dr NT Vandehey, Department of Medical Physics, University of Wisconsin—Madison, Lawrence Berkeley National Laboratory, 1 Cyclotron Road, MS55R0121, Berkeley, CA 94720, USA.
E-mail: nickvandehey@gmail.com
Received 5 June 2009; revised 3 December 2009; accepted 4 December 2009; published online 30 December 2009

*et al*, 2004; Slifstein *et al*, 2004a), as well as the testing the validity of the cerebellum as a reference region (Asselin *et al*, 2007; Christian *et al*, 2004; Delforge *et al*, 1999; Olsson *et al*, 1999; Olsson *et al*, 2004).

For assessment of endogenous dopamine competition, it has been suggested that the radiotracer vascular transport rate constants, $K_1$ and $k_2$, have a significant effect on the sensitivity for detecting endogenous dopamine release (Morris and Yoder, 2006), despite these rate constants not being directly related to receptor binding. In a challenge-type experiment (i.e., amphetamine challenge), competitive dopamine release is evoked after administration of radioligand; it was simulated that $^{11}$C-raclopride yielded the highest sensitivity for detecting dopamine release in the striatum, as compared with other radiotracers, including $^{18}$F-fallypride, $^{11}$C-FLB457, and several other frequently used radioligands. The increased detection sensitivity was not attributed to the rate constants involved in specific binding of the radioligand to the receptor site, but rather to the tissue-to-plasma efflux rate constant, $k_2$. A fast $k_2$ constant provides rapid clearance of the radioligand from the free space after displacement by endogenous neurotransmitter, thus enhancing the change in the PET signal, which represents both bound and free states. However, in the case of extrastriatal $D_2/D_3$ receptor binding, $^{11}$C-raclopride does not have sufficient target-to-background signal to detect subtle changes in the specific binding. In these regions, higher-affinity radiotracers are required to provide a suitable signal from the specifically bound component of the PET measurement.

High affinity by itself is not sufficient for extrastriatal assay; a radiotracer must also have low nonspecific uptake, which is dependent on lipophilicity and nonspecific protein binding. This issue was illustrated by a semi-quantitative *in vivo* comparison of $^{11}$C-fallypride, $^{11}$C-FLB457 with $^{11}$C-cyclopropyl-FLB457 (Airaksinen *et al*, 2006). $^{11}$C-cyclopropyl-FLB457 has been investigated as a candidate radioligand for extrastriatal $D_2/D_3$ binding due to its high *in vitro* $D_2/D_3$ affinity, which is 10-fold greater than that of fallypride and FLB457 (Airaksinen *et al*, 2008). Semi-quantitative comparisons of these radiotracers showed similar target/cerebellum ratios in the subcortical and cortical regions, despite the significantly higher affinity of $^{11}$C-cyclopropyl-FLB457 for the $D_2/D_3$ receptors.

Designing and conducting PET experiments to separate and uniquely identify the radioligand delivery and binding components is challenging for a single bolus injection PET study. Frequently there is high covariance between the parameter estimates of delivery ($K_1$, $k_2$) and binding ($k_3$, $k_4$), particularly for high-affinity radiotracers with rapid specific binding ($k_3$). This high covariance limits the interpretation of each parameter independently. To effectively uncouple the *in vivo* parameters for the characterization of $^{18}$F-fallypride and $^{11}$C-FLB457, it is necessary to introduce several injections of ligand, each time varying the concentrations of unlabeled and radiolabeled ligand. These multiple-injection (MI) PET experiments methodologically perturb and observe the system to separate the high covariance between parameters by introducing competition between the labeled and unlabeled ligand for the receptor site (Morris *et al*, 2004).

MI PET strategies have been used for both FLB457 and fallypride to provide *in vivo* estimation of radioligand–receptor characteristics. Using the long-lived $^{76}$Br ($t_{1/2} = 16.1$ h) radiolabel, FLB457 has been evaluated in baboons for estimation of receptor density ($B_{max}$) (Delforge *et al*, 1999) and for assay of endogenous dopamine competition (Delforge *et al*, 2001). For $^{18}$F-fallypride, MI studies have been reported using rhesus monkeys for *in vivo* characterization (Christian *et al*, 2004) and using baboons for measurement of *in vivo* affinity (Slifstein *et al*, 2004a). It must be stressed that MI studies are uniquely designed to optimize the estimation of a particular parameter of interest. For example, an MI design occurring over several separate imaging sessions can yield estimates of the apparent affinity (through scatchard type of analysis) (Holden *et al*, 2002), but are often not suitable for uncoupling the radioligand transport parameters ($K_1$, $k_2$), which is possible with a single-session MI study. Thus, attempting to compare the *in vivo* characteristics of FLB457 and fallypride based on the literature findings is difficult because the experiments were not optimized for direct comparison.

The goal of this study was to perform a direct comparison of $^{18}$F-fallypride and $^{11}$C-FLB457 using the MI protocol in the rhesus monkey model. The experiments were designed to obtain estimates of both radioligand transport and binding parameters, with particular interest in the tissue-to-plasma efflux constant ($k_2$) and the *in vivo* equilibrium dissociation constant ($K_D$). Knowledge of these radioligand characteristics will aid in the design of future experiments with the goal of maximizing sensitivity to subtle differences in extrastriatal $D_2/D_3$ receptor binding and endogenous dopamine competition in applications for studying diseases where disruptions in the dopaminergic system are implicated.

## Materials and methods

### Chemical Synthesis of $^{18}$F-Fallypride and $^{11}$C-FLB457

The radionuclides were produced with an 11-MeV RDS 112 cyclotron (CTI, Knoxville, TN, USA). For obtaining $^{11}$C-FLB457, $^{11}$C was produced by static irradiation of 10% $H_2/N_2$, producing $^{11}$C-$CH_4$ in target and converted to $^{11}$C-methyl-triflate using an automated radiochemical system (Larsen *et al*, 1997). Labeling of FLB604 precursor and subsequent high-performance liquid chromatography (HPLC) separation were performed according to previously described methods (Lundkvist *et al*, 1998). For producing $^{18}$F-fallypride, a modified chemical-processing control unit (CPCU) was used for labeling of the tosyl-fallypride

precursor, as previously described (Mukherjee *et al*, 1995). After evaporation of the HPLC mobile phase, both $^{18}$F-fallypride and $^{11}$C-FLB457 were dissolved in 0.9% NaCl and passed through a 0.22-$\mu$m filter for injection. The precursors and reference standards were purchased from ABX (Radeberg, Germany). Specific activity of the radiotracers was determined using reference standards and analytic HPLC analysis.

For each study, a stock solution of either unlabeled FLB457 or unlabeled fallypride was prepared by dissolving a reference standard in a sterile 10% ethanol/saline solution. For the second and third injections of each experiment, a given volume of the stock solution was thoroughly mixed with the labeled radiotracer, lowering its specific activity as needed per the scan injection protocol.

## PET Scans

MI PET data were acquired from two male rhesus monkeys (*Macaca mulatta*; M1: 7 kg, 6 years; M2: 8 kg, 4 years) using the experimental designs described in Table 1. The experimental procedures were approved by the University of Wisconsin Institutional Animal Care and Use Committee. For the scanning procedure, the monkeys were initially anesthetized with ketamine (10 mg/kg, intramuscular) and maintained with 0.75% to 1.5% isoflurane for the entire duration of the scan. Atropine was administered intramuscularly at 0.25 mg to minimize secretions. Body temperature, breathing rate, heart rate, and $SpO_2$ levels were monitored and logged during the course of each scanning session. A catheter was placed in the saphenous vein for the administration of ligand and another was placed in the femoral artery for withdrawing arterial plasma samples.

The PET scans were acquired using a Concorde microPET P4 scanner (Tai *et al*, 2001), with the animal mounted in a custom head holder in the prone position. After positioning, attenuation scans were acquired for 518 secs using a $^{57}$Co transmission point source. Collection of emission data was initiated with the first bolus injection of radiotracer and continued throughout each of the multiple injections. After the scan, the animals were removed from the scanner bed and from anesthesia. On recovery of the swallowing reflex, the animals were returned to their home cage where they were monitored until they were alert.

## Input Function Determination

Arterial blood samples ($\sim$0.5 ml each) were drawn throughout the course of each study. The sampling frequency varied from 10 samples/minute after each injection to 0.1 samples/minute after 30 mins. The whole blood samples were mixed with heparinized saline and assayed for radioactivity using a 3″ NaI(Tl) well counter, cross-calibrated to the PET scanner. Blood samples were then centrifuged at 2200*g* for 5 mins and 250 $\mu$L plasma was extracted. The plasma samples were alkynized with 50 $\mu$L sodium bicarbonate before performing two ethyl acetate extractions (500 $\mu$L each) to extract the lipophilic species. Both extractions were combined and assayed and converted to radioactivity concentration units after applying a correction for extraction efficiency ($\sim$90%). The ethyl acetate was evaporated and thin-layer chromatography was performed to assess the fraction of lipophilic plasma signal arising from lipophilic metabolites.

Whole blood and parent ligand plasma time–activity curves were then parameterized to an analytic function with three exponents to describe the decline of the radiotracer, as given in Figure 1A. Curve stripping was used to generate separate time courses corresponding to each injection subject to a constraint that the slowest component of decline was equal for all injections of each study. The parent ligand plasma time–activity data were converted to units of molar concentration (pmol/mL) through division by the injected specific activity. A decay correction was

**Table 1** Experimental design

| *Animal/experiment*<br>*Tracer* | *M1a*<br>*$^{18}$F-fallypride* | *M2a*<br>*$^{18}$F-fallypride* | *M1b*<br>*$^{11}$C-FLB457* | *M2b*<br>*$^{11}$C-FLB457* | *M1c*<br>*$^{11}$C-FLB457* |
|---|---|---|---|---|---|
| Monkey scan day[a] | 0 | 166 | 16 | 0 | 220 |
| $t_1$ (mins) | 0 | 0 | 0 | 0 | 0 |
| $a_1$ (MBq) | 130 | 120 | 120 | 120 | 60 |
| $m_1$ (nmol) | 2.0 | 0.7 | 1.8 | 0.7 | 1.0 |
| $SA_1$ (GBq/$\mu$mol) | 67 | 170 | 67 | 180 | 59 |
| $t_2$ (mins) | 100 | 100 | 30 | 40 | 100 |
| $a_2$ (MBq) | 120 | 110 | 130 | 130 | 130 |
| $m_2$ (nmol) | 13.1 | 10.6 | 11.6 | 12.8 | 11.4 |
| $SA_2$ (GBq/$\mu$mol) | 9.3 | 10.3 | 10.7 | 9.6 | 11.5 |
| $t_3$ (mins) | 150 | — | 60 | 81 | 150 |
| $a_3$ (MBq) | 47 | — | 12 | 19 | 117 |
| $m_3$ (nmol) | 100 | — | 109 | 102 | 111 |
| $SA_3$ (GBq/$\mu$mol) | 0.5 | — | 0.1 | 0.2 | 1.1 |
| $t_{end}$ (mins) | 180 | 150 | 120 | 121 | 182 |
| Estimated maximum receptor occupancy (%) | 13%, 64%, 98% | 12%, 77% | 38%, 97%, 100% | 19%, 94%, 100% | 23%, 98%, 100% |

[a]Monkey scan day represents number of days after the monkey's first MI study.

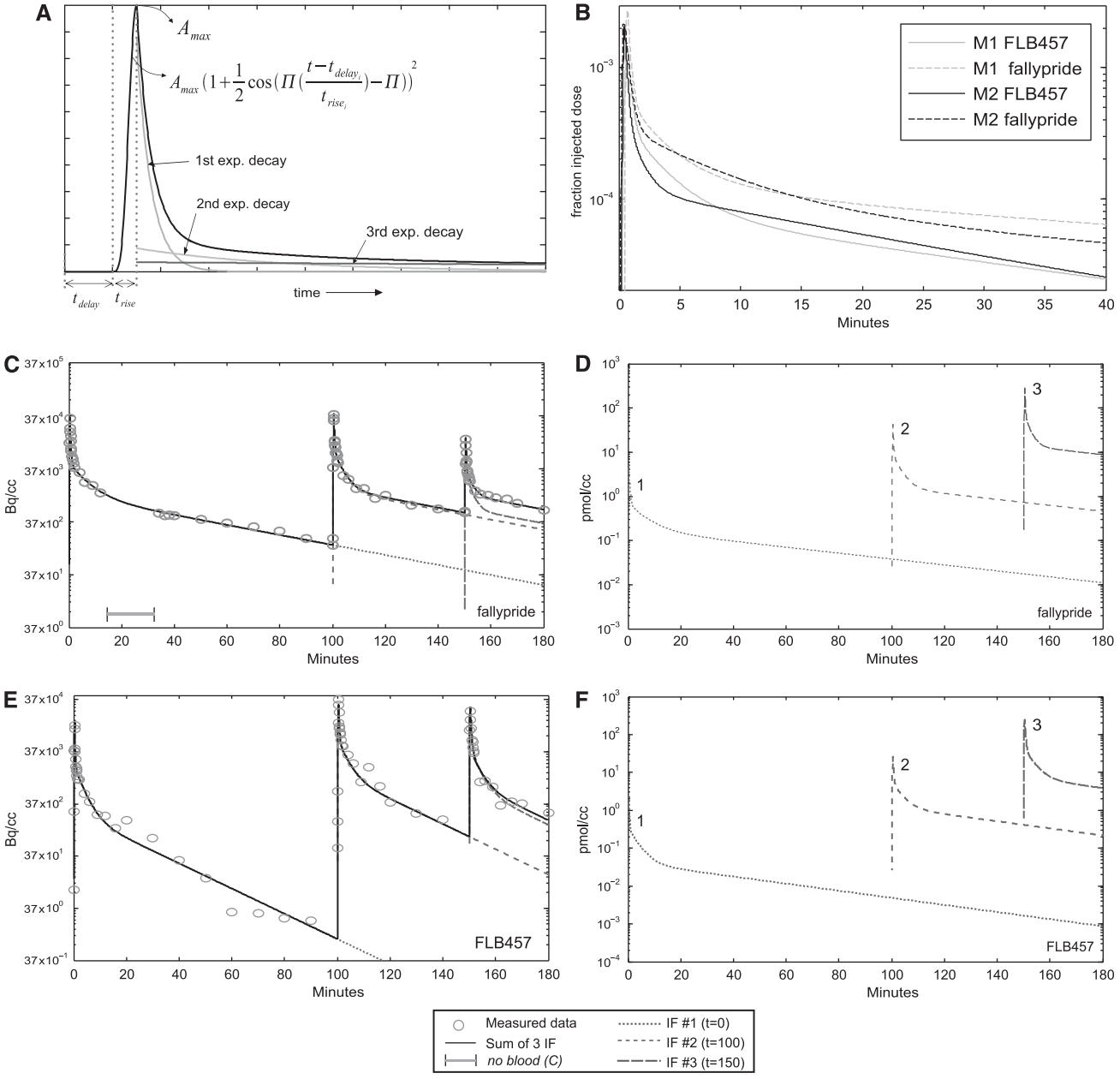


**Figure 1** Model input function description and fitting results. (**A**) The model input function used in fitting the measured input functions. (**B**) Fraction of the injected dose, time shifted to $t = 0$. Each curve represents the average of all injections of a particular study. The dotted lines are for fallypride, solid lines are for FLB457. (**C**) The measured input function radioactivity from the M1a fallypride study (circles) and the fit of measured data, as fit with three separate input functions (dotted lines) and the sum of the three input functions (solid line). The horizontal bar indicates the time period where no blood samples were drawn due to an obstructed arterial draw line. (**D**) Three input functions scaled by specific activity, shown in pmol/cc (M1a fallypride). (**E**, **F**) Same as in panels **C** and **D**, but for FLB457 (M1c).

applied to the molar concentration to represent the 'cold' ligand, which does not undergo radioactive decay.

## Image Processing

The PET list mode data were binned into sinograms with durations of 30 seconds per frame, with corrections applied for scanner deadtime and random coincidence events. Emission sinograms were reconstructed with filtered backprojection using a $0.5\,cm^{-1}$ ramp filter, zoom of 1.5, and $128 \times 128 \times 63$ voxel matrix size with a voxel size of $1.26\,mm \times 1.26\,mm \times 1.21\,mm$, with corrections applied for attenuation, scanner normalization, and scatter to create images with quantitative units. The data were not decay-corrected, as radioactive decay is accounted for in the model.

The reconstructed time series for each monkey were spatially transformed into a common space for generation

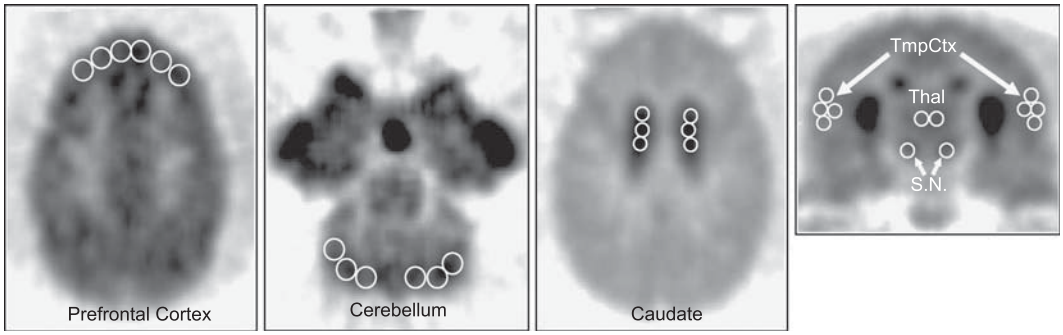


**Figure 2** Representative locations of ROIs over the six regions used for analysis. ROIs are shown on a single slice ($^{18}$F-fallypride, 5 to 20 mins), but were drawn on multiple adjacent slices.

of regional time–activity curves. A rigid-body registration was performed to the integrated images of $^{11}$C-FLB457 and $^{18}$F-fallypride using the FSL flirt software, and the affine transformation was applied to the entire dynamic PET series (Smith *et al*, 2004). Regions of interest (ROIs) were centrally placed within the boundaries of each region on the integrated PET image and applied to the dynamic time series for each study. Time–activity curves were obtained for the general regions of the thalamus, substantia nigra (SN), temporal cortex, prefrontal cortex, caudate, and cerebellum. The ROI placement for each region is shown in Figure 2. The thalamus region (0.13 cm$^3$) was placed predominantly over the medial dorsal portion of the thalamus; the SN (0.14 cm$^3$) over the pars compacta and other SN sub-regions unidentifiable in PET images; the temporal cortex region (TmpCtx) (0.87 cm$^3$) represented the superior temporal sulcus; and the frontal cortex region (1.26 cm$^3$) encompassed the dorsal prefrontal cortex (PFC). The caudate time–activity data were also incorporated into the parameter estimation process (although not for estimation of receptor density). The caudate (caud) region was defined over the central area of the caudate head using a volume of 0.16 cm$^3$. No distinction was made between left and right regions. The cerebellum ROI (cbm) (0.63 cm$^3$) was drawn over the cortex of the cerebellar lobes and positioned to avoid signal from the white matter, vermis, and surrounding regions.

## Optimization of Experimental Design

A single-session, MI design using the labeled–unlabeled model describes the *in vivo* kinetics of the ligands (Delforge *et al*, 1990). The MI experiments were designed with the goal of yielding optimal parameter identifiability for the PET model parameters describing plasma–tissue transport [$K_1$, $k_2$] and ligand–receptor binding [$f_{ND}k_{on}$, $k_{off}$, $B_{max}$] (Innis *et al*, 2007), with special focus on regions of low binding, such as the cortex. The protocol design involved a multiple-step optimization procedure, first using sensitivity analysis and then Monte Carlo (MC) methods. Initial designs investigated protocols with three serial injections of radiolabeled and unlabeled ligand. The entire experimental design was constrained to be less than 3 hours.

Sensitivity analysis was performed to determine the injection protocol that maximizes the determinant of the reduced hessian matrix ($H_R$) based on the preliminary parameter estimates reported for $^{18}$F-fallypride (Christian *et al*, 2004) and $^{76}$Br-FLB457 (Delforge *et al*, 1999), using arterial plasma input functions obtained from preliminary studies. Only binding parameters ($f_{ND}k_{on}$, $B_{max}$, $k_{off}$) were included in $H_R$. The parameters for the optimization algorithms included injection times for the second and third injections as well as the radioactivity and mass injected for each of the three injections. The optimization was performed to select the protocols that yielded the highest parameter precision in the $H_R$.

MC simulations were then performed to assess the effects of noise on parameter precision and to examine the sensitivity for estimation of $K_1$ and $k_2$, which were not included in $H_R$ during the initial sensitivity analysis. These simulations were performed by simulating 100 instances of MI PET curves, adding noise to the simulated data, $ROI_{model}$, using a noise model similar to a previously published method (Logan *et al*, 2001):

$$ROI_*(t) = ROI_{\text{model}}(G(0,1))^* c_1\sqrt{ROI_{\text{model}}}) + G(0,1))^* c_2$$

Subscripts '*' and '*model*' represent simulated noise-added and pre-noise (simulated) data, and $G(0,1)$ represents a normally distributed random number with mean 0 and standard deviation 1. Constants $c_1$ (0.5 to 2.5) and $c_2$ (0 to 75) represent noise levels, each adjusted to mimic the noise level of the ROI being simulated. The noisy simulated data ($ROI_*(t)$) were fit using methods as described below. The protocol with fits giving the most accurate and precise estimation of the input parameters was used for the PET scanning sessions.

Both sensitivity analysis and MC simulations were repeated before each PET scanning session, using refined starting estimates based on measured data from earlier studies. After the initial $^{18}$F-fallypride study (M1a), the optimization protocol was revised, leading to the second $^{18}$F-fallypride study (M2a) using a protocol with only two injections. After the first $^{11}$C-FLB457 study (M1b), the transport ($K_1$, $k_2$) and $k_{off}$ estimates were updated for the sensitivity analysis procedures. The sensitivity analysis results suggested multiple protocols that were further examined using the MC methods, leading to selection of a new protocol for M2 (M2b) with an increase in the time between injections. After acquisition of the

second $^{11}$C-FLB457 study, the protocol was revised in the same manner leading to another protocol for a third $^{11}$C-FLB457 experiment (M1c), which was slightly adjusted to match the timing in M1a. The experimental protocols used for the multiple-injection (MI) studies are given in Table 1.

### Multiple Injection (MI) Model

*Model Description*: For MI experiments with three injections ($i = 1, 2, 3$), there are a total of three differential equations describing the rate of change of the free ligand concentration (dF/dt) and another three differential equations describing bound (dB/dt) ligand concentration, which are as below:

$$\frac{dF_i}{dt} = K_1 C_{p_i} - k_2 F_i - f_{ND} k_{on} (B_{max} - \sum_i B_i) F_i + k_{off} B_i$$

$$\frac{dB_i}{dt} = f_{ND} k_{on} (B_{max} - \sum_i B_i) F_i + k_{off} B_i$$

These six differential equations share the same values for the plasma-to-tissue rate constant ($K_1$), tissue-to-plasma efflux constant ($k_2$), the ligand–receptor association ($f_{ND}k_{on}$), dissociation ($k_{off}$) rate constants, and receptor density ($B_{max}$). The molar concentration of the ligand in the arterial plasma ($C_{pi}$) for each injection serves as the input function to the model. The output signal measured by the PET scanner ($Model_j$) is related to the state variables by the equation:

$$Model_j = \frac{1}{t^j_{end} - t^j_{begin}} \int_{t^j_{begin}}^{t^j_{end}} \left\{ \sum_i [SA_i(t)(1 - F_V)(F_i(t) + B_i(t))] + F_V C_{WB}(t) \right\} dt$$

with $j$ dynamic PET frames and specific activity injection of $SA_i$ for each injection, and $t_{begin}$ and $t_{end}$ the beginning and ending times of each frame, respectively. The blood-borne component in each region is modeled as the whole blood time course ($C_{WB}(t)$) multiplied by the fractional blood volume ($F_V$), which was set at $F_V = 0.04$.

*Parameter Estimation*: The following assumptions were used in an effort to increase parameter identifiability in these regions of the brain with varying levels of dopamine $D_2/D_3$ receptors:

(i) Both $^{18}$F-fallypride and $^{11}$C-FLB457 were assumed to bind to the same set of $D_2/D_3$ receptors in the brain. Thus, receptor density $B_{max}$ was constrained to a single value for both radiotracers.
(ii) The *in vivo* association ($k_{on}$) and dissociation ($k_{off}$) rate constants, and the non-displaceable (ND) free fraction ($f_{ND}$) are uniform across the examined brain regions for both radiotracers.

Model configuration and parameter estimation were performed using the COMKAT software algorithms (Muzic and Cornelius, 2001). A constrained non-linear search using the Levenberg–Marquardt optimization algorithm was performed for estimation of the kinetic parameters. The parameter estimates were made both on an individual ROI basis and simultaneously in multiple regions using an objective function that minimized the total sum of squares residual, *RSS*, across $N$ ROIs consisting of $J$ frames each, as given below.

$$RSS(p) = \sum_{n=1}^{N} \sum_{j=1}^{J} w_{n,j} (PET_{n,j} - Model_{n,j})^2$$

Depending on what parameters we were trying to estimate, a subset of the $p$ was used, where $p = [f_{ND}k_{on}, k_{off}, [K_{1_n}, K_{2_n}, B_{max_n}]_n]$. Uniform weighting ($w_{n,j} = 1$) was used for all of the frames (which were of equal duration) (Muzic and Christian, 2006). All rate constants ($K_1$, $k_2$, $f_{ND}k_{on}$, $k_{off}$) were constrained to fall within the bounds of [0,1] ($min^{-1}$, $ml\,cm^{-3}\,min^{-1}$). $B_{max}$ was constrained to [0,100] ($nmol\,L^{-1}$).

Estimation of the individual rate constants was performed in a stepwise manner, incorporating the assumptions outlined above, following these three steps:

*Step 1. Determination of $k_{off}$:* The identifiability of $k_{off}$ is greatest in the regions of the brain with high specific receptor binding, particularly during the period of radioligand displacement. The PET time series from the caudate, thalamus, and SN were used to obtain the estimate of $k_{off}$, using the parameter set $p = [f_{ND}k_{on}, k_{off}, [K_{1_n}, K_{2_n}, B_{max_n}]_n]$ and $n = 1,2,3$ for these regions. It should be noted that in the caudate, only $k_{off}$ could be sufficiently uncoupled from the other parameters and this region was not used for estimation of the other parameters. These methods provided a single $k_{off}$ value for each individual study (and radiotracer).

Step 2. *Determination of regional $B_{max}$:* The PET time series from the thalamus, SN, PFC, and TmpCtx were then used for estimation of the parameter set $p = [f_{ND}k_{on}, [K_{1_n}, K_{2_n}, B_{max_n}]_n]$, using a fixed value for $k_{off}$ as determined from Step 1. Thus $f_{ND}k_{on}$ was constrained to be uniform across all brain regions, whereas regional differences were accounted for by differing receptor density and plasma transport rates. A mean $B_{max}$ was then obtained for each brain region based on an average of the data obtained from the $^{18}$F-fallypride and the $^{11}$C-FLB457 studies.

Step 3. *Determination of $f_{ND}k_{on}$ and regional $K_1$, $k_2$:* Using fixed values for $k_{off}$ and $B_{max}$, the PET time series was then used for the final estimation of

$$p = [f_{ND}k_{on}\,[K_{1_n}, K_{2_n}]_n]$$

The apparent equilibrium dissociation constant was then calculated for each radiotracer in each monkey as follows: $K_{Dapp} = k_{off}/f_{ND}k_{on}$.

*Fitting Cerebellum Data*: In the cerebellum, the rate constants were determined using both a one-compartment model (1CM) and a two-compartment model (2CM). For 1CM fitting, we used $p = [K_1, k_2]$ and for 2CM fitting we used $p = [K_1, k_2, B_{max}]$, with $f_{ND}k_{on}$ and $k_{off}$ fixed to values determined using the methods described above from the other brain regions. The Akaike Information Criterion (Akaike, 1974) was calculated for comparing the models to examine whether the presence of the additional term for receptor density ($B_{max}$) in the 2CM model was justified.

### Estimation of Uncertainty

Uncertainty in parameter estimates was performed using MC methods similar to those described by Salinas *et al* (2007). Noise-free data were first simulated on the basis of the implemented experimental protocols and final parameter estimates. Noise was then added in a manner identical as described in the optimization section. A total of 65 trials were run for each radiotracer (five ROIs each). Multi-step fitting procedures were used as described above. The standard deviation (s.d.) and mean of the parameter estimates across trials were calculated to give a coefficient of variation (COV = s.d./mean).

## Results

### Input Function Determination

The results of the input function fitting procedure for the M1 $^{18}$F-fallypride study are shown in Figures 1C–1F. Figure 1B shows a comparison of the arterial plasma time–activity curves of parent radioligand for $^{11}$C-FLB457 and $^{18}$F-fallypride. The data are normalized to the injected dose and shown for the first 40 mins after injection and averaged over the three injections. These plots show that native $^{11}$C-FLB457 was cleared from the arterial plasma faster than native $^{18}$F-fallypride. The fraction of parent compound was 2 to 4 times higher for $^{18}$F-fallypride than for $^{11}$C-FLB457 at approximately 5 mins after injection. The faster rate of clearance of $^{11}$C-FLB457 continued throughout the course of the study, with the slowest exponential component of 0.033 $min^{-1}$ for $^{11}$C-FLB457 and 0.017 $min^{-1}$ for $^{18}$F-fallypride, on average.

### Optimization of Experimental Design

Using MC methods, it was found that the identifiability of $K_1$ and $k_2$ was not affected by the experimental design within the range of schemes required for $f_{ND}k_{on}$, $k_{off}$, and $B_{max}$ identifiability. For $^{18}$F-fallypride, the parameter identifiability could be achieved with only two injections, thus the saturating dose (injection-3) was eliminated from the fallypride protocol for M2. For $^{11}$C-FLB457, the initial parameter estimates used for optimization led to a protocol with injection times at 0, 30, and 60 mins (see Table 1). This preliminary study did not adequately identify $B_{max}$ and $f_{ND}k_{on}$, yielding a correlation between parameter estimates greater than 0.9. To better identify $f_{ND}k_{on}$ and $B_{max}$, this protocol was then refined by increasing the time interval between the injections for the second and third $^{11}$C-FLB457 experiments.

### Parameter Estimates

Of the specific binding parameters $f_{ND}k_{on}$, $B_{max}$, and $k_{off}$; identifiability was greatest for $k_{off}$, showing a small covariance with the other parameters. $k_{off}$ was found to be slower for $^{11}$C-FLB457 than for $^{18}$F-fallypride, with an average value of 0.016 $min^{-1}$ and 0.022 $min^{-1}$, respectively (Table 2). As indicated in the methods, the estimate of $k_{off}$ was best for M1b due to the long period of scanning after the third injection, but other parameters were most identifiable from the M1c study. Accordingly, the M1 $^{11}$C-FLB457 results presented in Table 2 represent an average of data from M1b and M1c.

All of the experiments for $^{11}$C-FLB457 and $^{18}$F-fallypride showed high identifiably for both transport parameters and ligand–receptor interaction parameters, with the exception of $f_{ND}k_{on}$ for $^{11}$C-FLB457 for M2. For this study, a range of estimates for $f_{ND}k_{on}$ and $k_{off}$ are reported that provided similarly acceptable fits to the data, with the average values reported in Table 2. Within this range estimates for $f_{ND}k_{on}$ and $k_{off}$, $K_1$ and $k_2$ were largely unaffected, due to the small covariance between the parameters of transport and binding. When averaged across both monkeys, $K_{Dapp}$ for $^{18}$F-fallypride is found to be higher than that of $^{11}$C-FLB457 (0.39 nmol/L versus 0.13 nmol/L). Figure 3A shows an example of the measured PET data and the model fit to the data.

The precision of the parameter estimates is given as COV, as derived by MC-based methods. For $^{11}$C-FLB457 fits, the most precise COVs were for $K_1$ and $k_2$ estimates (2%), followed by $B_{max}$ (6%), $k_{off}$ (9%), and $f_{ND}k_{on}$ (12%). The error associated with $^{18}$F-fallypride estimates gave COVs of 4% for $K_1$ and $k_2$, 5% for $B_{max}$, and 3% for $f_{ND}k_{on}$ and $k_{off}$.

### Cerebellar Kinetics

The parameter estimates for cerebellar data are shown in the bottom of Table 2. An example of the data fit for M1 is shown in Figure 3B, comparing both 2CM and 1CM models. For both $^{11}$C-FLB457 studies, the 2CM model provided the most appropriate fit using the Akaike information criterion, which is visually evident in Figure 3B. For $^{18}$F-fallypride, the 1CM model was adequate for describing the data. It was also found that $^{11}$C-FLB457 showed considerably higher ND volume of distribution, $V_{ND}$ ($= K_1/k_2$), than $^{18}$F-fallypride; primarily attributable to the lower $k_2$ of $^{11}$C-FLB457. This difference in $V_{ND}$ holds for both 1CM and 2CM models.

## Discussion

The motivation for this study was to perform a direct comparison of the kinetics of two commonly used PET radioligands for assaying extrastriatal $D_2/D_3$ binding, $^{18}$F-fallypride and $^{11}$C-FLB457. Although a single-bolus-injection experimental design is most feasible for studying changes in receptor–ligand binding (through DVR or $BP_{ND}$) in humans, such a design cannot uncouple the individual transport and binding processes of the radiotracer. We have chosen to implement this experimentally complex protocol

**Table 2** Results of fitting procedures

| | | | *M1* | | *M2* | |
|---|---|---|---|---|---|---|
| | | | *$^{18}$F-fallypride M1a* | *$^{11}$C-FLB457 M1b+M1c* | *$^{18}$F-fallypride M2a* | *$^{11}$C-FLB457 M2b* |
| | $f_{ND}k_{on}$ | nmol/L/min | 0.046 | 0.13 | 0.080 | 0.15[a] |
| | $k_{off}$ | min$^{-1}$ | 0.024 | 0.014 | 0.021 | 0.018[a] |
| | $k_{Dapp}$[b] | nmol/L | *0.52* | *0.11* | *0.25* | *0.15*[a] |
| PFC | $K_1$ | ml/cm$^3$/min | 0.22 | 0.49 | 0.55 | 0.53 |
| | $k_2$ | min$^{-1}$ | 0.37 | 0.13 | 0.46 | 0.20 |
| | $B_{max}$ | nmol/L | 0.6 | | 0.4 | |
| TMP | $K_1$ | ml/cm$^3$/min | 0.43 | 0.51 | 0.58 | 0.53 |
| | $k_2$ | min$^{-1}$ | 0.53 | 0.14 | 0.52 | 0.21 |
| | $B_{max}$ | nmol/L[1] | 0.6 | | 0.4 | |
| Thalamus | $K_1$ | ml/cm$^3$/min | 0.42 | 0.66 | 0.76 | 0.66 |
| | $k_2$ | min$^{-1}$ | 0.49 | 0.18 | 0.68 | 0.25 |
| | $B_{max}$ | nmol/L | 1.5 | | 0.8 | |
| SN | $K_1$ | ml/cm$^3$/min | 0.35 | 0.36 | 0.41 | 0.40 |
| | $k_2$ | min$^{-1}$ | 0.54 | 0.10 | 0.53 | 0.19 |
| | $B_{max}$ | nmol/L | 3.0 | | 2.3 | |
| Cbm (2CM) | $K_1$ | ml/cm$^3$/min | 0.57 | 0.65 | 0.51 | 0.53 |
| | $k_2$ | min$^{-1}$ | 0.71 | 0.24 | 0.56 | 0.21 |
| | $B_{max}$ | nmol/L | 0.0 | **0.4** | 0.0 | **0.1** |
| | $V_{ND}$[c] | ml/m$^3$ | *0.8* | ***2.7*** | *0.9* | ***2.5*** |
| Cbm (1CM) | $K_1$ | ml/cm$^3$/min | **0.57** | 0.64 | **0.51** | 0.51 |
| | $k_2$ | min$^{-1}$ | **0.71** | 0.22 | **0.54** | 0.19 |
| | $V_T$ [d] | ml/cm$^3$ | ***0.8*** | *2.9* | ***0.9*** | *2.7* |

Abbreviations: Cbm, cerebellum; 1CM, one-compartment model; 2CM, two-compartment model; PFC prefrontal cortex; SN, substantia nigra; TMP, temporal cortex.

The values in bold indicate values the most appropriate model, based on the Akaike Information Criterion.

[a]The values reported for M2 FLB are averages of estimates in a range $k_{on} = 0.1$ to 0.2, $k_{off} = 0.010$ to 0.025, and $K_{Dapp} = 0.1$ to 0.2.

[b]$K_{Dapp} = k_{off}/f_{ND}k_{on}$. This is a calculated value based on $f_{ND}k_{on}$ and $k_{off}$, and was not a parameter included in the fit to the data.

[c]$V_{ND} = K_1/k_2$ for 2CM. This is a calculated value based on $K_1$ and $k_2$, and was not a parameter included in the fit to the data.

[d]$V_T = V_{ND} = K_1/k_2$ for 1CM. This is a calculated value based on $K_1$ and $k_2$, and was not a parameter included in the fit to the data.

to directly compare and characterize the *in vivo* rate constants of $^{11}$C-FLB457 and $^{18}$F-fallypride to guide experimental design for future studies and to evaluate the strengths and weaknesses of each radiotracer for extrastriatal $D_2/D_3$ assessment.

## Plasma Analysis

Measurements show that $^{11}$C-FLB457 is removed from the blood much more quickly than $^{18}$F-fallypride. Rapid metabolism and clearance of radioligand from the plasma could be advantageous as it permits a shorter scanning duration to achieve a stable measure of receptor binding. However, the accuracy of the measured arterial concentration is greatly diminished due to low counting statistics due to the short half-life of the $^{11}$C radiolabel.

The rapid metabolism for both tracers resulted in hydrophilic species, which did not cross the blood–brain barrier. At later time points the lipophilic metabolites were present in the ethyl acetate extraction along with the parent compound as assayed by thin-layer chromatography. The fraction of non-parent lipophilic species did not exceed 20% for either radiotracer at the time prior to subsequent injection. However, the uncertainty in this measurement was high, particularly for $^{11}$C-FLB457, and corrections for the presence of these radiolabeled species were not applied to the input functions. Previous analysis of MI experiments has shown that with MI protocols involving multiple injections of radioligand, the presence of the lipophilic fraction had a negligible effect on the parameter estimates because the relative proportion remained small with the addition of parent compound at each injection (Christian *et al*, 2004). These effects of lipophilic metabolites on the parameter estimates were further examined for both $^{18}$F-fallypride and $^{11}$C-FLB457 through simulations of various levels of lipophilic metabolites. As a greater fraction of lipophilic plasma concentration was attributed to lipophilic metabolites

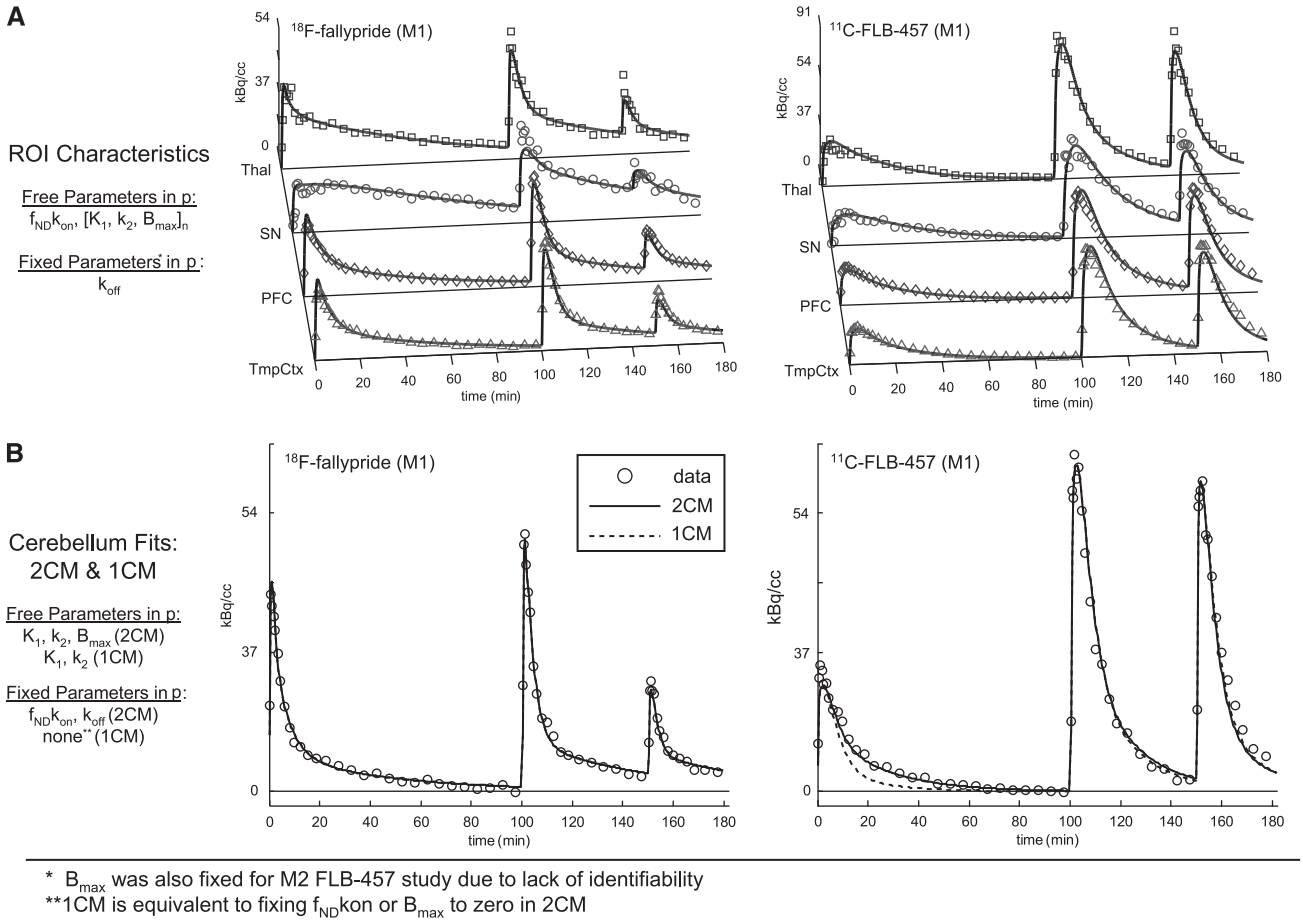


**Figure 3** Representative time–activity curves and model estimations. (**A**) A summary of model estimation and measured data for the thalamus, SN, prefrontal cortex, and temporal cortex (in M1). (**B**) A summary of cerebellar data fits with both 1CM and 2CM models. The 1CM is represented by a dotted line and the 2CM is shown with a solid line. The measured data have been re-binned from a 30-secs frame duration into longer frame durations for illustrative purposes only.

(up to the extreme case of a 50% lipophilic metabolites at 100 mins), the associated change in kinetic parameter estimates was only significant in $f_{ND}k_{on}$ and resulted in an approximately 10% reduction in this parameter.

## Optimization of Experimental Design

MI experiments must be properly designed for the injection timing and the proportion of radiolabeled and unlabeled compound to yield estimated parameters that are uniquely identified. However, MI optimization procedures present a challenge because the procedures used require *a priori* information about the transport and binding characteristics of a tracer when the goal of the experiments is to determine these very parameters. On the basis of our previous experience with $^{18}$F-fallypride (Christian *et al*, 2004), it was possible to achieve excellent identification of all the parameters with $^{18}$F-fallypride in both animals. The results of the first $^{18}$F-fallypride study (M1a) led to elimination of the third injection for the second study (M2a) on the basis of a robust design-optimization strategy described by Salinas *et al* (2007). Finding a protocol giving good parameter estimation for $^{11}$C-FLB457 was not so straightforward. We acquired two scans (M1b, M2b) with poor identifiability for $f_{ND}k_{on}$ and $B_{max}$ before finding a protocol that was able to sufficiently identify these parameters of binding (M1c). This was achieved by increasing the interval between the injections to provide additional data, which were needed to adequately uncouple the delivery and rapidly binding processes.

## Model Assumptions

Several constraints were enforced to increase the identifiability of the estimated *in vivo* rate constants (by minimizing the total number of simultaneously estimated parameters). For $^{11}$C-FLB457 and $^{18}$F-fallypride, the ligand–receptor association ($k_{on}$)

and dissociation ($k_{off}$), and the ligand-free fraction ($f_{ND}$) were assumed to be uniform across all regions of the brain for each individual. This assumption of a uniform apparent $K_D$ across brain regions also implies that synaptic dopamine concentration is uniform across regions. The estimation of $k_{off}$ can be made with high precision ($\sim$3%) in the brain regions where the PET signal is dominated by the specifically bound compartment, which is visually evidenced by displacement of radioligand after saturating doses of ligand. This was the motivation for including the region of the caudate for the estimation of $k_{off}$ only. To further validate the use of a uniform $k_{off}$, each of the regions (caudate, thalamus, SN) were first fit independently for $k_{off}$ and the resulting estimates were all within 30% of the shared value. Consistent estimates of $k_{off}$ across medium- and high-density $D_2/D_3$ regions have also been previously reported for these radiotracers (Delforge *et al*, 1999, Christian *et al*, 2004). In the low-receptor-density regions, the use of a fixed $k_{off}$ serves to minimize the coupling with the transport and forward binding constants. The assumption of uniform $f_{ND}$ across regions is commonly assumed in all PET methods of analysis using a reference region to account for the ND compartment (e.g., $BP_P$ and $BP_{ND}$) (Innis *et al*, 2007). As a result, the constraints of $f_{ND}k_{on}$ and $k_{off}$ across all regions of the brain will yield a uniform apparent $K_D$ for each radioligand.

The concentration of receptor sites available for binding ($B_{max}$) was also constrained to be equal for $^{11}$C-FLB457 and $^{18}$F-fallypride. To accommodate this assumption, both radiotracers must not only have high selectivity for the $D_2/D_3$ receptors, but also possess a similar ratio of $D_2$ and $D_3$ affinities. *In vitro* comparisons of $D2_{long}$ and D3 affinities have been reported for fallypride ($Ki_{D2long}$:$Ki_{D3}$ = 2.2 nmol/L: 1.6 nmol/L) and FLB457 ($Ki_{D2long}$:$Ki_{D3}$ = 0.65 nmol/L: 0.42 nmol/L) using $^3$H-spiperone, thus showing a consistent relation for both ligands (Stark *et al*, 2007). Some discrepancy was reported when comparing the $D2_{short}$ and $D2_{long}$ isoform affinities between fallypride ($Ki_{D2long}$:$Ki_{D2short}$ = 2.2 nmol/L:2.1 nmol/L) and FLB457 ($Ki_{D2long}$:$Ki_{D2short}$ = 0.65 nmol/L:1.6 nmol/L). In our data, there was no apparent bias for the estimation in the region of the SN, believed to consist predominantly of $D2_{short}$ receptors (Kahn *et al*, 1998), by assuming an identical $B_{max}$ for $^{11}$C-FLB457 and $^{18}$F-fallypride binding, and the constraint was applied to be consistent with the other brain regions. Accordingly, the constrained values for $B_{max}$ were similar to the values as derived independently (i.e. M1 SN $B_{max}$: fallypride = 2.8 nmol/L, FLB457 = 3.3 nmol/L, average = 3.0 nmol/L).

### Regional Binding and Transport

Examination of the results show that the main differences between radiotracers lie in their affinity for $D_2/D_3$ receptors and the rate at which they clear out of tissue from the free space. Using the averages of both studies, we report an apparent $K_D$ (*in vivo*, $K_{Dapp} = k_{off}/f_{ND}k_{on}$) of 0.39 nmol/L for $^{18}$F-fallypride and 0.13 nmol/L for $^{11}$C-FLB457. This three-fold difference can be attributed to the combination of faster binding and slower dissociation of $^{11}$C-FLB457 as compared with that of $^{18}$F-fallypride. This difference is relatively consistent, with a twofold difference in humans (Narendran *et al*, 2009) and *in vitro* measures of $K_D$ (0.030 nmol/L versus 0.018 nmol/L) (Halldin *et al*, 1995; Mukherjee *et al*, 1995) and $K_i$ (2.2 nmol/L versus 0.65 nmol/L, using $^3$H-spiperone) for fallypride and FLB457, respectively. For fallypride, the measured apparent dissociation constant is in close agreement with 0.38 nmol/L from previous studies using the rhesus monkey (Christian *et al*, 2004), but lower than 1.3 nmol/L as reported for the baboon (Slifstein *et al*, 2004a). For FLB457, the literature values have been reported as 0.21 nmol/L for the baboon (Delforge *et al*, 1999) and 0.35 nmol/L and 0.9 nmol/L for humans (Olsson *et al*, 2004; Suhara *et al*, 1999).

The delivery of the parent compound from the plasma to the free space of the tissue ($K_1$) was similar for both radiotracers, yielding a mean of $K_1 = 0.48 \pm 0.15$ mL/cm$^3$/min for $^{18}$F-fallypride and $K_1 = 0.54 \pm 0.10$ mL/cm$^3$/min for $^{11}$C-FLB457 when averaged across all brain regions. However, there was a large difference in the tissue-to-plasma efflux constant, $k_2$, with values of $0.54 \pm 0.10$ min$^{-1}$ for $^{18}$F-fallypride and $0.18 \pm 0.05$ min$^{-1}$ for $^{11}$C-FLB457. On the basis of these findings, it is seen that the ND distribution volume ($V_{ND} = K_1/k_2$) is more than three-fold larger for $^{11}$C-FLB457 than $^{18}$F-fallypride: 3.0 mL/cm$^3$ as compared with 0.9 mL/cm$^3$. This measure of $V_{ND}$ for $^{18}$F-fallypride is consistent with our previous findings using the rhesus monkey through the MI approach (Christian *et al*, 2004). For $^{76}$Br-FLB457, previous MI experiments reported a $V_{ND}$ of 0.35 mL/cm$^3$ for the baboon (Delforge *et al*, 1999). Recent studies of humans found a $V_{ND}$ of 2.9 mL/cm$^3$ for $^{11}$C-FLB457 (Asselin *et al*, 2007), which is in closer agreement with the value reported here. This large discrepancy in $V_{ND}$ for FLB457 may be species or methodology dependent; however, it does emphasize the importance of performing radioligand comparisons on the same subjects.

The significant difference in $V_{ND}$ between $^{11}$C-FLB457 and $^{18}$F-fallypride may, in part, be due to the higher lipophilicity of fallypride. Generally, higher lipophilicity produces a reduction in the free compound in both the plasma ($f_p$) and brain tissue ($f_{ND}$), and $V_{ND}$ depends on the ratio of these fractions at equilibrium. On the basis of literature values using HPLC measurement, $^{18}$F-fallypride has a log $k_w$ = 2.43 (Mukherjee *et al*, 1995) and $^{11}$C-FLB457 has a log $k_w$ = 1.89 (Schmidt *et al*, 1994). *In silico* measurements support the higher lipophilicity of fallypride, with an average log *P*-value of 3.3 for fallypride and 2.9 for FLB457, as calculated using ALOGPS (Tetko and Yu, 2005).

### Effect of $k_2$ Differences

One of the primary differences in the *in vivo* behavior of $^{11}$C-FLB457 and $^{18}$F-fallypride is the tissue-to-plasma efflux constant ($k_2$). For $^{11}$C-FLB457, the approximately threefold reduction in $k_2$ results in a significantly higher signal in the ND compartment, frequently measured in the cerebellum. Such an increase in this component of the PET signal is advantageous for radiotracers that require an extended PET scanning duration to achieve $BP_{ND}$ stability by improving the statistics in the PET signal. On the basis of the examination of M1 in this study, it was found that at 80 mins after injection, the decay-corrected $^{11}$C-FLB457 study yielded a cerebellar concentration that was 70% greater than that in the $^{18}$F-fallypride study, despite having a plasma concentration that was 85% less than that of $^{18}$F-fallypride. This increased signal in the ND compartment also improves visualization of the cortical regions, which can aid in the definition of ROIs or in spatial co-registration or normalization. However, as the signal-to-noise ratio is dependent on measured counts (and not decay corrected counts), this advantage of increased $V_{ND}$ is lost for $^{11}$C-FLB457 as compared with $^{18}$F-fallypride, due to its shorter half-life of the radiolabel.

The $k_2$ parameter also plays a role in the sensitivity of a radioligand for measuring changes in endogenous dopamine competition. Through use of computer simulations, Morris and co-workers performed a detailed comparison of prospective radioligands available for measuring dopamine transmission in the brain (Morris and Yoder, 2006). In their survey of these radiotracers, it was found that fallypride was almost three-fold more sensitive than FLB457 to dopamine displacement. In the case of dopamine displacement, the radioligand is administered prior to a manipulation (i.e. administration of amphetamine), which induces the release of endogenous dopamine, and in turn displaces the radiotracer from the specifically bound receptors. For displacement experimental designs, the PET detection sensitivity of a radioligand will be enhanced by rapid dissociation ($k_{off}$) and tissue clearance ($k_2$), thus enhancing the contrast in the PET signal before and after dopamine release. For dopamine displacement experiments, the faster kinetics of fallypride will improve detection sensitivity, but only in regions where sufficiently high PET signal is present. A recent study by Narendran *et al* (2009) directly compared $^{11}$C-fallypride- and $^{11}$C-FLB457-measured $BP_{ND}$ changes before and after endogenous dopamine competition in humans using an amphetamine challenge. Their results found that $^{11}$C-FLB457 showed 30% to 70% higher sensitivity (through $\Delta BP_{ND}$) to dopamine competition than $^{11}$C-fallypride in the cortical regions of the brain. In contrast to the 'displacement'-type study, this 'blocking'-type study is designed to have the competing dopamine present prior to the administration of the radioligand. This difference in study design favors $^{11}$C-FLB457 for the blocking-type experiment, because this design is less sensitive to the combination of slow binding dissociation, increased PET signal in both the specifically bound and ND states, and the higher proportion in the specifically bound state relative to the ND state.

### Cerebellar Kinetics

The radiotracer kinetics in the cerebellum are of great importance for PET $D_2/D_3$ receptor studies because it is commonly used as a reference region in $BP_{ND}$ determination. In this study, it was found that significant specific binding could be measured in the cerebellum for $^{11}$C-FLB457 but not for $^{18}$F-fallypride.

The presence of specific $D_2/D_3$ binding in cerebellum has been frequently reported in the literature for $^{11}$C-FLB457 (Asselin *et al*, 2007; Delforge *et al*, 1999; Olsson *et al*, 2004), leaving one to conclude that similar issues with specific cerebellar binding would be present with $^{18}$F-fallypride. The inability of fallypride to detect specific cerebellar binding in this study can be explained, in part, by its lower *in vivo* affinity when compared with FLB457. A $\sim 3\times$ higher apparent $K_D$ of fallypride will result in a $3\times$ lower bound-to-ND fraction at equilibrium. However, the insensitivity to cerebellar binding is also attributed to several other characteristics of fallypride, including the reduced radiotracer clearance from the blood, faster $k_2$, and slower rate of receptor–ligand association ($f_{ND}k_{on}$) as compared with FLB457.

To investigate the sensitivity of both tracers to a small level of cerebellar binding, we compared simulations of the cerebellum-to-plasma ratios for both radiotracers assuming a receptor density of 0.1 nmol/L, as shown in Figure 4. In the absence of specific binding, this ratio should plateau at $V_{ND}$. In the presence of specific binding, the ratio will plateau at $V_T$ ($= V_{ND} + V_S$) (as simulated in Figure 4). The distinctive upward bend in the $^{11}$C-FLB457 curve is due to the fast $f_{ND}k_{on}$ combined with the rapidly declining plasma concentration. It can be seen that this shape in the curve is enhanced by the slower $k_2$ and $k_{off}$ of $^{11}$C-FLB457. Thus, the slow clearance of $^{11}$C-FLB457 from the tissue acts as a leaky integrator of the radiotracer, enhancing the opportunity for the ligand to specifically bind to the receptor sites. This shape is not seen with $^{18}$F-fallypride because of the combination of slower plasma clearance of the parent ligand, a slower rate of specific binding, and faster dissociation from specific binding sites.

When using a reference region method of analysis, such as the Logan DVR graphical method, specific cerebellar binding will result in an underestimation of $BP_{ND}$, with the following relationship between measured $BP_{ND}$ and true $BP_{ND}$ being derived:

$$\frac{BP_{ND_{measured}}}{BP_{ND_{true}}} = \left[1 - \frac{B_{max_{ref}}(1 + BP_{ND_{tissue}})}{B_{max_{tissue}}(1 + BP_{ND_{ref}})}\right]$$

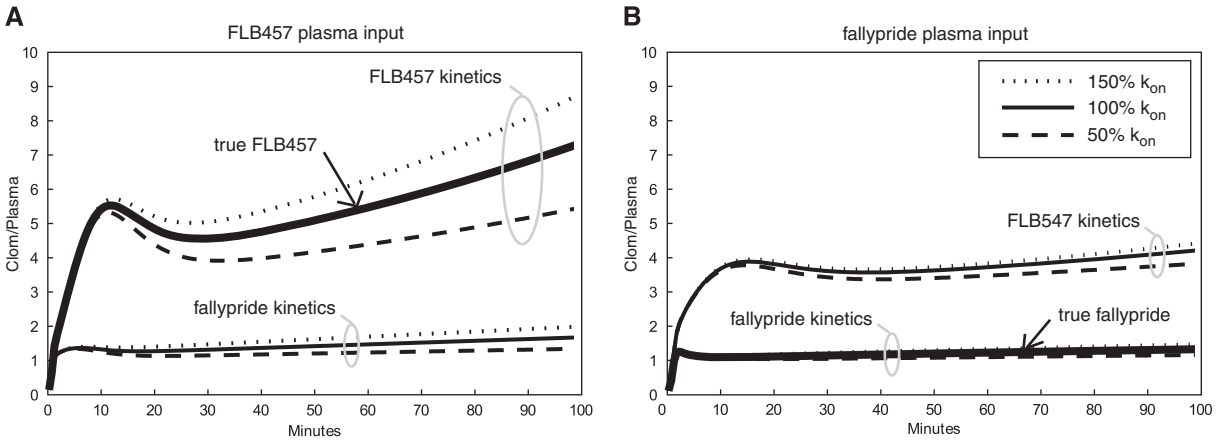


**Figure 4** Cerebellum-to-parent plasma ratios assuming a cerebellar $D_2/D_3$ receptor concentration of 0.1 nmol/L. (**A**) Simulated cerebellum/plasma curves using FLB457 measured plasma input function; (**B**) curves generated using measured $^{18}$F-fallypride plasma concentration. Both fallypride-like kinetics and FLB457-like kinetics are represented using each plasma input function. Variations in $k_{on}$ from the tracer's true $k_{on}$ value (±50%) are shown by dotted and dashed lines. The thick solid lines indicate the kinetics parameters of FLB457, with a FLB457 input function (**A**) and fallypride kinetic parameters and fallypride input (**B**).

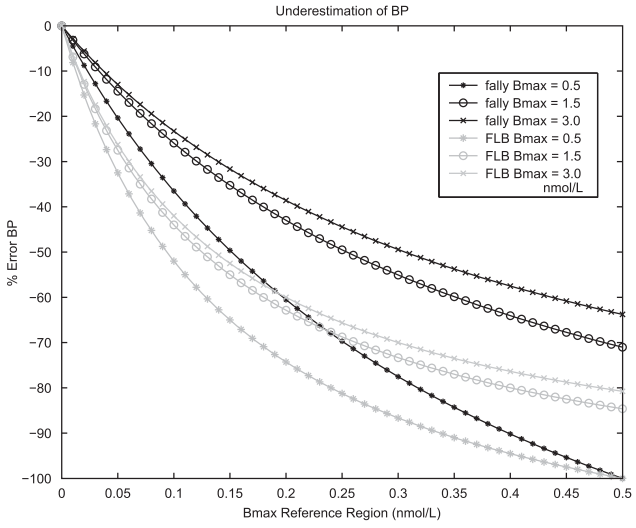


**Figure 5** Theoretical underestimation of $BP_{ND}$ using reference region methods. The series of plots are the theoretical regions of the cortex (*, $B_{max} = 0.5$ nmol/L), thalamus (○, $B_{max} = 1.5$ nmol/L), and SN (×, $B_{max} = 3.0$ nmol/L). Fallypride curves are black; FLB457 curves are gray.

The effect of specific binding in the cerebellum on the measurement of $BP_{ND}$ is shown in Figure 5, where the higher degree of underestimation for FLB457 can be attributed to its higher affinity. Of primary importance is the non-linearity in bias in the low-density regions where the receptor density is only slightly greater than that found in the cerebellar lobes. Across a cohort of animals with variable levels of cerebellar binding, this will result in high variability of $BP_{ND}$ estimation in low-receptor-density regions such as the cortex. We have recently reported high variability in cortical $^{18}$F-fallypride binding (in $BP_{ND}$) in a large cohort of rhesus monkeys (Christian *et al*, 2009), which may be a direct consequence of cohort variation in cerebellar $D_2/D_3$ receptor concentration. The extent and variability of $D_2/D_3$ density in the cerebellum (lobes) in the population is not known, and thus it is not possible to assess the variability in $BP_{ND}$ due to cerebellar specific binding. Without knowledge of specific cerebellar binding, caution must be used in interpreting binding in low-density regions when reference region methods are employed.

## Conclusions

There is a high degree of similarity in the visual appearance of the PET images of $^{18}$F-fallypride and $^{11}$C-FLB457, with both radiotracers yielding similar target-to-background ratios throughout the brain regions, with differing $D_2/D_3$ receptor densities. However, assessing the performance of a radiotracer simply on the basis of target-to-background ratios can lead to a misguided understanding of a radiotracer's ability to provide an accurate measure of receptor–ligand binding (Eckelman *et al*, 2009). Compared with fallypride, FLB457 shows faster ligand–receptor binding and slower dissociation from the receptor, translating into an equilibrium dissociation constant that is approximately three times lower. Fallypride clears from the ND space faster and remains in the plasma longer than FLB457. The higher affinity and ND component of FLB457 will provide higher tracer uptake in the cortical and cerebellar regions; however, this will be offset by lower counting statistics when using a $^{11}$C radiolabel. These properties suggest that $^{18}$F-fallypride is better suited for endogenous displacement-type experiments. For reference region methods of analysis, both radiotracers will suffer from potential $BP_{ND}$ bias in the low binding regions.

The presence of cerebellar binding may preclude the use of reference region methods for cortical $D_2/D_3$ assay.

## Acknowledgements

We acknowledge the help provided by Dr Todd Barnhart and Jon Engle in radiotracer preparation; Liz Ahlers in data acquisition; and Leslie Resch, Allison Theide, and Julie Larson in animal handling. This work was supported by funding through NCI T32 CA009206-30, NIH T90 DK070079, NIH/NIBIB EB006110, and NIAAA RO1 AA12277.

## Disclosure/conflict of interest

The authors declare no conflict of interest.

## References

Airaksinen AJ, Finnema SJ, Nag S, Mukherjee J, Gulyas B, Halldin C (2006) A new PET radioligand 11C cyclopropyl-FLB 457 for imaging extrastriatal dopamine D2 receptors: evaluation in monkey and comparison to 11C FLB 457 and 11C fallypride. *Neuroimage* 31:T15-T

Airaksinen AJ, Nag S, Finnema SJ, Mukherjee J, Chattopadhyay S, Gulyás B, Farde L, Halldin C (2008) [11C]Cyclopropyl-FLB 457: a PET radioligand for low densities of dopamine D2 receptors. *Bioorg Med Chem* 16:6467–73

Akaike H (1974) A new look at the statistical model identification. *Automatic Control, IEEE Transact Biomed Eng* 19:716–23

Asselin MC, Montgomery AJ, Grasby PM, Hume SP (2007) Quantification of PET studies with the very high-affinity dopamine D-2/D-3 receptor ligand [C-11]FLB 457: re-evaluation of the validity of using a cerebellar reference region. *J Cereb Blood Flow Metab* 27:378–92

Christian BT, Narayanan T, Shi B, Morris ED, Mantil J, Mukherjee J (2004) Measuring the *in vivo* binding parameters of [18F]-fallypride in monkeys using a PET multiple-injection protocol. *J Cereb Blood Flow Metab* 24:309–22

Christian BT, Vandehey NT, Fox AS, Murali D, Oakes TR, Converse AK, Nickles RJ, Shelton SE, Davidson RJ, Kalin NH (2009) The distribution of D2/D3 receptor binding in the adolescent rhesus monkey using small animal PET imaging. *Neuroimage* 44:1334–44

Delforge J, Syrota A, Mazoyer BM (1990) Identifiability analysis and parameter-identification of an *in vivo* ligand–receptor model from PET data. *IEEE Transact Biomed Eng* 37:653–61

Delforge J, Bottlaender M, Loc'h C, Guenther I, Fuseau C, Bendriem B, Syrota A, Mazière B (1999) Quantitation of extrastriatal D2 receptors using a very high-affinity ligand (FLB 457) and the multi-injection approach. *J Cereb Blood Flow Metab* 19:533–46

Delforge J, Bottlaender M, Pappata S, Loc'h C, Syrota A (2001) Absolute quantification by positron emission tomography of the endogenous ligand. *J Cereb Blood Flow Metab* 21:613–30

Eckelman WC, Kilbourn MR, Mathis CA (2009) Specific to nonspecific binding in radiopharmaceutical studies: it's not so simple as it seems!. *Nucl Med Biol* 36:235–7

Halldin C, Farde L, Högberg T, Mohell N, Hall H, Suhara T, Karlsson P, Nakashima Y, Swahn CG (1995) Carbon-11-FLB 457: a radioligand for extrastriatal D2 dopamine receptors. *J Nucl Med* 36:1275–81

Holden JE, Jivan S, Ruth TJ, Doudet DJ (2002) *In vivo* receptor assay with multiple ligand concentrations: an equilibrium approach. *J Cereb Blood Flow Metab* 22: 1132–41

Innis RB, Cunningham VJ, Delforge J, Fujita M, Gjedde A, Gunn RN, Holden J, Houle S, Huang S-C, Ichise M, Iida H, Ito H, Kimura Y, Koeppe RA, Knudsen GM, Knuuti J, Lammertsma AA, Laruelle M, Logan J, Maguire RP, Mintun MA, Morris ED, Parsey R, Price JC, Slifstein M, Sossi V, Suhara T, Votaw JR, Wong DF, Carson RE (2007) Consensus nomenclature for *in vivo* imaging of reversibly binding radioligands. *J Cereb Blood Flow Metab* 27:1533–9

Kahn ZU, Mrzljak L, Gutierrez A, de la Calle A, Goldman-Rakic PS (1998) Prominence of the dopamine D2 short isoform in dopaminergic pathways. *Proc Natl Acad Sci USA* 95:7731–6

Larsen P, Ulin J, Dahlstrom K, Jensen M (1997) Synthesis of [11C]iodomethane by iodination of [11C]methane. *Appl Radiat Isot* 48:153–7

Logan J, Fowler JS, Volkow ND, Ding YS, Wang G-J, Alexoff DL (2001) A strategy for removing the bias in the graphical analysis method. *J Cereb Blood Flow Metab* 21:307–20

Lundkvist C, Sandell J, Nagren K, Pike VW, Halldin C (1998) Improved syntheses of the PET radioligands, [C-11]FLB457, [C-11]MDL100907 and [C-11]beta-CIT-FE, by the use of [C-11]methyl triflate. *J Labelled Compounds Radiopharm* 41:545–56

Morris E, Yoder K (2006) Positron emission tomography displacement sensitivity: predicting binding potential change for positron emission tomography tracers based on their kinetic characteristics. *J Cereb Blood Flow Metab* 27:606–17

Morris ED, Christian BT, Yoder KK, Muzic RF (2004) Estimation of local receptor density, B'max, and other parameters via multiple-injection positron emission tomography experiments. *Methods Enzymol* 385: 184–213

Mukherjee J, Yang Z-Y, Das M, Brown T (1995) Fluorinated benzamide neuroleptics—III Development of (S)-*N*-[(1-allyl-2-pyrrolidinyl)methyl]-5 (3-[18F]fluoropropyl) 2,3-dimethoxybenzamide as an improved dopamine D-2 receptor tracer. *Nucl Med Biol* 22:283–96

Mukherjee J, Yang Z-Y, Brown T, Lew R, Wernick M, Ouyang X, Yasillo N, Chen C-T, Mintzer R, Cooper M (1999) Preliminary assessment of extrastriatal dopamine d-2 receptor binding in the rodent and nonhuman primate brains using the high affinity radioligand, 18F-fallypride. *Nucl Med Biol* 26:519–27

Mukherjee J, Christian BT, Narayanan TK, Shi B, Collins D (2005) Measurement of d-amphetamine-induced effects on the binding of dopamine D-2/D-3 receptor radioligand, 18F-fallypride in extrastriatal brain regions in non-human primates using PET. *Brain Res* 1032:77–84

Muzic RF, Cornelius S (2001) COMKAT: compartment model kinetic analysis tool. *J Nucl Med* 42:636–45

Muzic RF, Christian BC (2006) Evaluation of objective functions for estimation of kinetic parameters. *Med Phys* 33:342–53

Narendran R, Frankle WG, Mason NS, Rabiner EA, Gunn RN, Searle GE, Vora S, Litschge M, Kendro S, Cooper TB, Mathis CA, Laruelle M (2009) Positron emission tomography imaging of amphetamine-induced dopamine release in the human cortex: a comparative evaluation of the high affinity dopamine D2/3 radiotracers [11C]FLB 457 and [11C]fallypride. *Synapse* 63:447–61

Okauchi T, Suhara T, Maeda J, Kawabe K, Obayashi S, Suzuki K (2001) Effect of endogenous dopamine on endogenous dopamine on extrastriated [(11)C]FLB 457 binding measured by PET. *Synapse* 41:87–95

Olsson H, Halldin C, Swahn CG, Farde L (1999) Quantification of [11C]FLB 457 binding to extrastriatal dopamine receptors in the human brain. *J Cereb Blood Flow Metab* 19:1164–73

Olsson H, Farde L (2001) Potentials and pitfalls using high affinity radioligands in PET and SPET determinations on regional drug induced D2 receptor occupancy—a simulation study based on experimental data. *Neuroimage* 14:936–45

Olsson H, Halldin C, Farde L (2004) Differentiation of extrastriatal dopamine D2 receptor density and affinity in the human brain using PET. *Neuroimage* 22:794–803

Riccardi P, Baldwin R, Salomon R, Anderson S, Ansari MS, Li R, Dawant B, Bauernfeind A, Schmidt D, Kessler R (2008) Estimation of baseline dopamine D2 receptor occupancy in striatum and extrastriatal regions in humans with positron emission tomography with [18F] fallypride. *Biol Psychiatry* 63:241–4

Salinas C, Muzic JRF, Ernsberger P, Saidel GM (2007) Robust experiment design for estimating myocardial beta adrenergic receptor concentration using PET. *Med Phys* 34:151–65

Schmidt DE, Votaw JR, Kessler RM, Depaulis T (1994) Aromatic and amine substituent effects on the apparent lipophilicities of *N*-(2-pyrrolidinyl)methyl-substituted benzamides. *J Pharm Sci* 83:305–15

Slifstein M, Hwang D-R, Huang Y, Guo N, Sudo Y, Narendran R, Talbot P, Laruelle M (2004a) *In vivo* affinity of [18F]fallypride for striatal and extrastriatal dopamine D 2 receptors in nonhuman primates. *Psychopharmacology* 175:274–86

Slifstein M, Narendran R, Hwang DR, Sudo Y, Talbot PS, Huang Y, Laruelle M (2004b) Effect of amphetamine on [(18)F]fallypride *in vivo* binding to D(2) receptors in striatal and extrastriatal regions of the primate brain: single bolus and bolus plus constant infusion studies. *Synapse* 54:46–63

Smith SM, Jenkinson M, Woolrich MW, Beckmann CF, Behrens TE, Johansen-Berg H, Bannister PR, De Luca M, Drobnjak I, Flitney DE, Niazy RK, Saunders J, Vickers J, Zhang Y, De Stefano N, Brady JM, Matthews PM (2004) Advances in functional and structural MR image analysis and implementation as FSL. *Neuroimage* 23(Suppl 1):S208–19

Suhara T, Sudo Y, Okauchi T, Maeda J, Kawabe K, Suzuki K, Okubo Y, Nakashima Y, Ito H, Tanada S, Halldin C, Farde L (1999) Extrastriatal dopamine D2 receptor density and affinity in the human brain measured by 3D PET. *Int J Neuropsychopharmacol* 2:73–82

Stark D, Piel M, Hubner H, Gmeiner P, Grunder G, Rosch F (2007) *In vitro* affinities of various halogenated benzamide derivatives as potential radioligands for non-invasive quantification of D-2-like dopamine receptors. *Bioorg Med Chem* 15:6819–29

Tai YC, Chatziioannou A, Siegel S, Young J, Newport D, Goble RN, Nutt RE, Cherry SR (2001) Performance evaluation of the microPET P4: a PET system dedicated to animal imaging. *Phys Med Biol* 46:1845–62

Tetko IV, Tanchuk VY (2005) ALOGPS (http://www.vcclab.org) is a free online program to predict lipophilicity and aqueous solubility of chemical compounds. *Proceedings of the 229th National Meeting of the American Chemical Society*, San Diego, CA, 13–17 March 2005